Electronic Structure of Self-Assembled Amorphous Polyfluorenes

Svetlana Kilina, Enrique R. Batista, Ping Yang, Sergei Tretiak, Avadh Saxena, Richard L. Martin, and Darryl L. Smith*

Theoretical Division, Center for Nonlinear Studies (CNLS), and Center for Integrated Nanotechnologies (CINT), Los Alamos National Laboratory, Los Alamos, New Mexico 87545

ABSTRACT We investigate the role of conformational disorder and intermolecular interactions on the electronic structure of amorphous clusters of polyfluorenes. Classical molecular dynamics simulations are used to determine probable molecular geometries and chain packing, and first-principles density functional theory calculations are employed to determine electronic structure and orbital localization properties. Intramolecular and intermolecular effects are disentangled by contrasting results for densely packed oligomer clusters and for ensembles of isolated oligomers with the same intramolecular geometries. Our simulations show that intermolecular disorder allows for nearly planar configurations of interacting fluorenes compared to the isolated molecules. This rationalizes the experimentally detected formation of the planar crystalline morphologies that frequently accompany twisted glassy configurations in fluorene films. The energy gap (HOMO—LUMO gap) significantly decreases for planar configurations. The electron and hole orbital energies are strongly dependent on both torsional angles and intermolecular interactions. This leads to strong localization of electronic states in amorphous polymer aggregates, which is analyzed by examining the respective orbital participation ratios. Notably, the energies of unoccupied levels show stronger dependence on the conformational disorder, compared to that of occupied levels. This results in the more probable formation of trap states near the edge of the conduction band than near the valence band.

KEYWORDS: conjugated polymers · disordered systems · electronic structure · charge localization · organic semiconductors

Photoluminescent polymers are technologically important materials. The tunability of the color of light emission *via* chemical synthesis, mechanical flexibility, solubility, and low-cost fabrication promise a number of technological advantages over the traditional semiconductors.[1] Of all conjugated polymers, polyfluorenes, including poly-(9,9′-dioctylfluorene) (PFO), have attracted a special interest because of their efficient blue photoluminescence and one of the highest hole mobility values[2,3] (10^{-3} to 10^{-2} cm^2/Vs) in combination with excellent chemical and thermal stability.[4,5] These features render PFOs with great application potential as blue-light-emitting diodes (LED),[6,7] optical switches,[8] thin film transistors,[9] solar cells,[6] and lasers.[10]

A distinct structural feature, which is responsible for many unique physicochemical properties of fluorenes, is the presence of the bridging nonconjugated (sp^3) carbon atom between rigid planar biphenyl units (Figure 1b). This bridging atom can be functionalized by alkyl groups (or other radicals) to provide good solubility of the polymer without changing the principal features of electronic structure of the backbone.[4] The tetrahedral character of the sp^3-bonds of the bridging carbon allows for self-organization of PFO polymers into several distinct supramolecular structures at room temperature.[4] In films, PFO samples typically exhibit two morphological formations: amorphous glassy phase (α phase), in which PFO molecules have large torsional angles between the adjacent biphenyls, and the so-called β phase with a high degree of organization and planar PFO molecules.[5,11,12] A strong variation of film morphology leads to a vast difference in photophysics of PFO materials. For example, β-phase PFOs reveal red-shifted absorption and emission spectra with higher polarizabilities.[11,12] It was also experimentally[3,13] and theoretically[14] found that charge carrier mobility is higher in the β phase compared to the glassy material. Packing also determines the exciton binding energy:[15] measurements in well-oriented samples show values of the binding energy almost ten times smaller than those in disordered films.[15,16]

These features demonstrate an important role of disorder in determining electronic properties of organic semiconductors.[12,17–19] However, unlike inorganic semiconductors, disorder in the conjugated polymers is not associated with broken chemical bonds. Disorder in PFO materials, has two general origins: Intramolecular conformations lead to variations in bond-lengths, torsional angles, and

*Address correspondence to dsmith@lanl.gov.

Received for review April 1, 2008 and accepted June 02, 2008.

Published online June 14, 2008.
10.1021/nn800204m CCC: $40.75

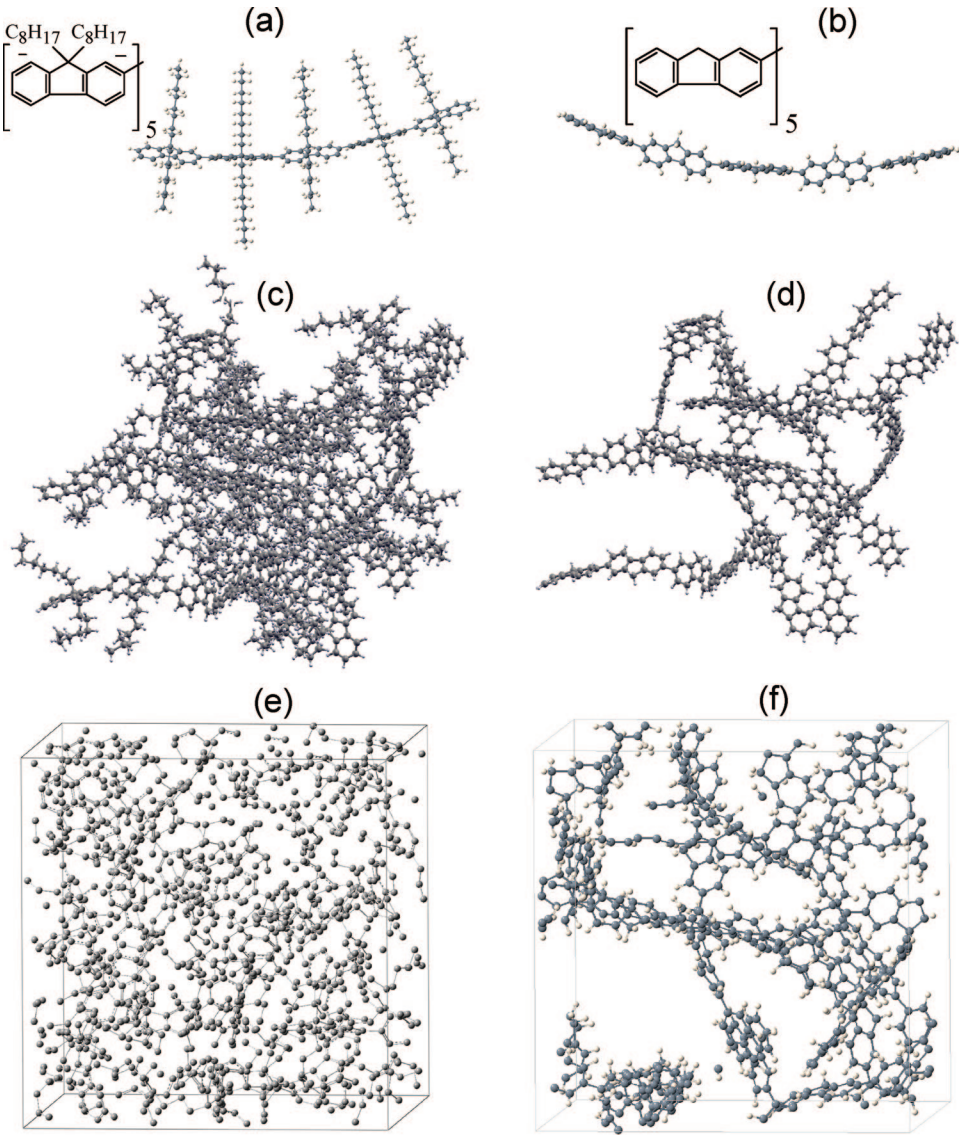

Figure 1. Calculated structures of PFO polymers with (left panels) and without (right panels) octyl groups C_8H_{17}. Panels a and b show chemical structure (inserts) and an optimal geometry of an isolated PFO pentamer. Panels c–f display a representative snapshot of an amorphous phase of the polymer aggregate containing eight PFO chains in a periodically repeated simulation cell of ~3 × 3 × 3 nm^3 size. PFO chains extending over the boundary of the periodic box are shown in two different ways: To preserve visual continuity of PFO molecules, panels c and d display such PFO chains as imaginary replicas into the next periodic cell; to visualize materials structure, panels e and f project such PFO chains to the opposite side of the same simulation cell.

appearance of on-chain defects, whereas intermolecular interactions arise from material morphology, chain alignment, and packing. The interplay between these effects and their influence on the electronic structure, optical, and transport properties of PFO materials is not clear yet.

On the other hand, efficient material development requires microscopic information on the relationship between structural and physical properties. It is extremely challenging to separate features originating from inter- or intramolecular interactions unambiguously in experiments. Consequently, theoretical analysis of electronic structure, morphology, the interplay between different types of disorder, and effect of this interplay on localization/delocalization of electronic states in amorphous PFO aggregates is of current topical interest. Most of existing theoretical work has been focused on the characteristics of optical and transport properties of isolated PFO oligomers,[5,20,21] with few efforts on studying intermolecular interactions in crystalline packing.[14,22–24] Unfortunately, simulations of realistic disordered materials as used in devices are scarce.[19] The main reason is the computationally unmanageable number of atoms in realistic amorphous polymer systems. The accurate first principles molecular modeling techniques, such as density functional theory (DFT), are costly, limiting the application to relatively small systems (hundreds of atoms). Particularly, simulations of dynamics and packing of the material are extremely expensive with *ab initio* methods. The approaches for larger systems include Monte Carlo and classical force field (FF) calculations. Here the computational results are derived from model potentials, which allow description of the molecular framework and interactions. However, such parameters are hard to determine for complex systems, thus making the accuracy of FFs problematic. Besides, this approach cannot provide information on the electronic structure of the system.

In this Article we investigate the role of intermolecular interactions and conformational disorder on the electronic structure of amorphous PFO materials. DFT parametrized FF potentials have been used to provide reliable geometries and packing morphologies for disordered polymers. Subsequent DFT calculations of selected snapshots give an accurate electronic structure of the amorphous material. Localization and delocalization properties of occupied and unoccupied electronic states are studied based on participation ratio analysis, an approach commonly used in inorganic semiconductors.[25] Our simulations show that the nature of the disorder and its impact on charge-carrier localization in

amorphous PFOs differ dramatically from those of disordered inorganic semiconductors, such as amorphous silicon. Electronic levels of disordered PFOs have mostly a localized character: partial charge density of the majority of states is distributed only over a few molecules, rather than spread over the entire cell. Thus, the bandlike delocalized description is not appropriate for amorphous fluorenes.

RESULTS AND DISCUSSION

The isolated PFO pentamer and one of the amorphous PFO samples we studied are shown in Figure 1. The details of sample preparation can be found in the Methodology section. Figure 2a shows that the optimal torsional angle between biphenyl groups in the isolated PFO chain is 37°. An identical minimum exists at 180° − 37° = 143° (not shown). Maxima of the torsional potential at planar (0° and 180°) and 90° configurations have a similar barrier height of about 0.13 eV (3 kcal/mol). As expected, packing chains into the material leads to a broad distribution of torsional angles.

Figure 2b displays a statistical analysis of the torsional angles in PFO molecules calculated for the 20 different amorphous samples and compares it with the Boltzmann distribution for torsional angles in the optimized isolated pentamer for three temperatures (300, 1000, and 2000 K). For each amorphous configuration (as an example, see the configuration in Figure 1d,f), the torsional angle, φ, between each pair of neighboring monomers of each PFO chain contributes to the statistical analysis shown in Figure 2b. The histogram distribution for amorphous samples follows well the Boltzmann function $\exp(-E_{tot}(\varphi)/(kT))$ predicted from the pentamer torsion curve (shown in Figure 2a) at 1000 K. Packing disorder weakly affects the optimal torsion angle in PFO chains: 40° and 140° remain the most probable values of the torsional angles. However, the distribution function for amorphous PFOs slightly deviates from the Boltzmann function, and shows asymmetry between 0° and 90° torsional angle distributions. Figure 2b evidences a broad variety of statistically viable angles (0°−60° and 120°−180°), particularly favoring planar conformations, which allow for optimal packing and π-stacking of the chains. A relatively high probability of PFO configurations with small torsional angles in interacting polymer systems rationalizes the presence of the β phase[12] that accompanies the glassy morphologies in the experimental thin films.

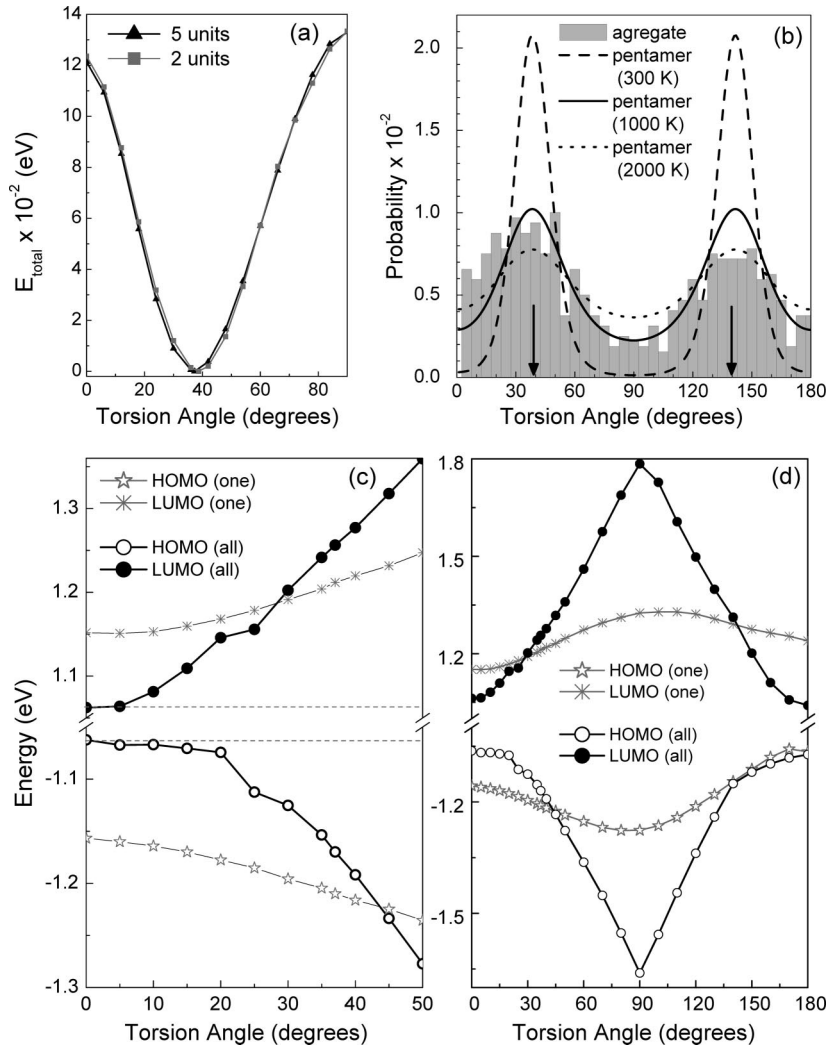

Figure 2. (a) Variation of electronic energy as a function of the torsional angle between two central monomers, calculated using B3LYP/6-31+G* for an isolated PFO dimer with octyl radicals (triangles) and a pentamer without octyl radicals (squares). (b) Comparison of torsional angle distribution in amorphous PFO aggregates and in the isolated pentamer. All distributions are normalized and the area under the curve is unitary. For the aggregates, probability distribution is calculated for 20 different amorphous samples after annealing (gray boxes). Black lines correspond to the probability distribution functions $\exp(-E_{tot}(\varphi)/(kT))$ predicted from the pentamer torsion curve shown in panel (a) at room temperature (dash line), at 1000 K (solid line), and at 2000 K (dot line). Arrows show the torsional angle in the optimized isolated pentamer at 0 K. Distribution of angles in amorphous PFOs slightly deviates from the Boltzmann distribution. (c,d) Variation of HOMO and LUMO energies in the isolated PFO pentamer as a function of the torsional angle. Circles correspond to data when all torsional angles are the same; stars describe the case when only a single torsional angle in the center of PFO varies, while the others hold the optimal angle of 37°. The dash line is used to emphasize the faster change of LUMO energy compared to HOMO for torsional angles <50°.

Variations in the torsional angles of the PFO lead to significant changes in the energies of the occupied and unoccupied electronic levels (Kohn−Sham orbitals), which, in turn, vary the respective energy gap value. Figure 2c shows the energy of HOMO and LUMO of an isolated PFO pentamer as a function of the torsion angle between nearest biphenyl rings. We consider two different cases: when all torsional angles have been changed simultaneously and when only one torsional

angle in the middle of the PFO chain has been varied, while all others have been fixed at the optimal 37° value. As expected, the HOMO−LUMO gap decreases for planar configurations providing optimal π overlaps. In contrast, the 90° conformation has the largest gap due to a disrupted π conjugation. These results correlate well with the red shift of the optical spectra of the β phase containing planar configurations of PFO molecules, compared to the α phase with randomly tilted PFO chains.[11,12]

Note that energies of occupied and virtual levels should exhibit similar behavior in simple electronic structure obtained by tight-binding calculations, owing to the symmetry between effective masses of electrons and holes imposed in this model. Interestingly, this is not the case in our calculations. Figure 2c demonstrates that at small angles (0°−40°), most probable in the PFO materials, the LUMO (electron orbital) energy changes more rapidly than HOMO (hole orbital) energy with variation of the torsional angle. Such a trend might lead to more probable trap states near the edge of unoccupied states, rather than near the edge of occupied states in the disordered PFO aggregates, hinting at a higher mobility of holes compared to electrons. Hereafter we refer to the occupied states as the valence band (VB) and the unoccupied states as the conduction band (CB). Nonetheless, because interchain interactions can change significantly the electronic structure of an amorphous system compared to an isolated molecule, the effects of inter- versus intrachain interactions on the electronic structure of amorphous PFO aggregates have to be analyzed as well.

Figure 3 compares the Kohn−Sham orbital energies in one of the equilibrium configurations of amorphous interacting PFOs with the noninteracting case. The noninteracting molecules (isolated PFOs) are obtained by removing all except one molecule from the simulation cell of the considered aggregate. Note that the geometry of each isolated PFO molecule is not optimized, but taken as it is from the amorphous snapshot and used for electronic structure computations. Because the number of atoms and the cell volume are identical for each noninteracting PFO, the absolute values of energy levels are calculated with respect to the same reference point in each molecule. Therefore, to obtain a noninteracting PFO system, calculated electronic states of each of the eight isolated PFO molecules are just combined together and shown as blue lines in Figure 3. To compare "interacting" and "noninteracting" cases, the zero energy is arbitrarily chosen to be in the middle of the energy gap of the aggregate for interacting chains and in the middle of the HOMO−LUMO gap of the noninteracting combined system. For the sample shown, the interchain interactions significantly decrease the energy gap of the aggregate compared to the noninteracting chains.

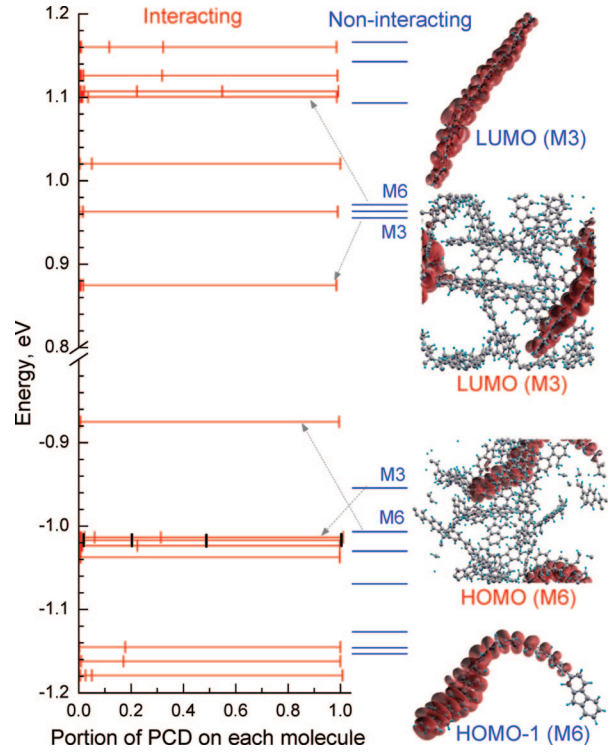

Figure 3. The left and middle panels show density of states for interacting (red) and noninteracting (blue) chains in one snapshot of amorphous PFOs. The *y*-axis represents the Kohn−Sham energies of single particle states with zero in the middle of the energy gap. Comparison of interacting and noninteracting PFOs reveals noticeable splittings and shifts of energies induced by interaction between molecules. In the interacting case (left), each horizontal line has a unitary length and is partitioned into eight intervals by small vertical lines. The length of each interval defines a percent P_{in} of the partial charge density (PCD) localized on each of the eight PFO molecules in the aggregate. For a given orbital *i*, if all but one of the intervals have a length close to zero, the PCD of the aggregate is localized on a single molecule. The more intervals with relatively large length, the stronger delocalization of the orbital. The right panel displays representative orbitals in amorphous (red labels) and isolated (blue labels) PFO pentamers (molecules M6 and M3) in one of the statistical samples. Note that other samples do not show the analogous trend for their HOMO and LUMO.

As expected, a molecule with the nearly planar conformation (marked by M3 in Figure 3) contributes to both LUMO and HOMO for the noninteracting case, since planar PFO molecules have the smallest energy gap among all other torsion configurations (see Figure 2c). However, in the aggregate, the LUMO and HOMO-1 (not HOMO) originate from the nearly planar molecule M3. While the energy difference between the HOMO-1 and LUMO of the aggregate is nearly equal to the energy gap (LUMO-HOMO) of the noninteracting molecule M3, the PFO with a V-shape (marked by M6 in Figure 3) contributes to the HOMO of the aggregate decreasing the energy gap by ~0.2 eV. The V-shape of the PFO molecule is due to a large torsional angle (70−90°) between the two central monomers. Such a large torsion is usually accompanied by localization of

the orbital on a part of the molecule. Indeed, examination of the respective orbitals shows a completely delocalized pattern for the nearly plane configuration M3 and localization for the V-shaped configuration M6 in the case of isolated molecules (right panel in Figure 3, blue labels). Moreover, the structure of these particular orbitals remains intact in the interacting sample (right panel in Figure 3, red labels). Although interchain interactions decrease the energy gap in most PFO aggregates, some of the amorphous samples show insignificant changes of the energy gap compared to those of noninteracting molecules. In addition, in some amorphous samples, the V-shaped molecules demonstrate an upward-shift of their energies with respect to other molecules in the aggregates (HOMO of the M6 is upshifted with respect to HOMO of the M3 in the aggregate shown in Figure 3), while in other amorphous samples, energies of the V-shaped molecules are either almost unchanged or experience a downward shift. Such a diversity points to a major role of neighboring PFOs that surround a V-shaped molecule in an aggregate, rather than a specific geometry of a single PFO chain.

We also note that the electronic states in the interacting samples are not always localized on a single chain. Instead of visual examination of each orbital, to this end we calculate a percent P_{in} of the partial charge density (PCD), $\rho_i = |\psi_i|^2$, for a specific Kohn−Sham orbital ψ_i, which is localized on the nth chain in the aggregate (see Supporting Information for computational details). This percentage is normalized, so that $\Sigma_{n=1}^{8} P_{in} = 1$. For each orbital i, the values of P_{in} are summed in the increasing order and shown in the left panel in Figure 3. Here each horizontal line is crossed by eight small vertical lines, which symbolize a portion, P_{in}, of the PCD on a specific molecule. This immediately provides us with detailed information on the orbital localization in the material. For example, P_{in} for i = HOMO-2, marked by black vertical lines in Figure 3, indicates the orbital delocalization over three molecules roughly contributing 20% ($x \approx 0.2$), 30% ($x \approx 0.5$), and 50% ($x \approx 1$) to the charge density, while the other five chains have a negligible contribution ($x \sim 0$). In contrast, both HOMO and LUMO have a very localized character, because only one molecule contributes to the charge distribution of these orbitals. By applying this approach to all 20 amorphous samples, we do not find specific patterns in PFO geometries that are responsible for the formation of delocalized states. Molecules with small and large torsion angles, planar and V-shaped configurations contribute equally to the delocalized states. However, we observe that PFO chains with nearly uniform torsions (10°−15° angle variation along the chain) have a much stronger tendency to create delocalized states than PFOs with a strong disorder in their torsion angles. Because of the broad distribution of torsional angles in the amorphous material (Figure 2b), many PFO chains in the aggregate have a very strong torsional disorder (typical variation of torsion angles is about 60°). Such disorder localizes the majority of electronic states on essentially a single chain. It is important to note that a few states close to the energy gap, including HOMO and LUMO, always have a completely localized character, and in all samples, LUMO and HOMO originate from the different molecules.

We next introduce the participation ratio (PR) and inverse participation ratio (IPR) to further understand delocalization of electronic states in amorphous PFO aggregates. The IPR (or PR) measure is commonly used in condensed matter physics to characterize disorder and localization in a bulk crystal of volume[26] V or in a discrete space (atoms)[25] (see Supporting Information). For an ideally localized state on a single atom PR = 1/IPR = 1. For a uniformly distributed wave function over all N atoms, PR = 1/IPR = N. We define PR in a molecular basis as

$$\mathrm{PR}(i) = \frac{\left(\sum_n P_{in}\right)^2}{\sum_n P_{in}^2} = \frac{1}{\sum_n P_{in}^2} \qquad (1)$$

where P_{in} is a portion of the PCD of the orbital i on the nth molecule (see Figure 3 and Supporting Information). Consequently, electronic states of a PFO aggregate that are completely localized on a single chain and delocalized over all eight molecules have PR = 1 and PR = N = 8, respectively.

Figure 4 shows both density of states (DOS) and PR as a function of energy for the combined 20 PFO aggregates and for a single amorphous sample (the same sample as shown in Figure 1d and Figure 3). The PR clearly demonstrates the existence of highly localized states not only near the band gap edges, but also deep inside the VB and the CB. Furthermore, there are no completely delocalized states; even states with very high and low energies do not show localization over more than 5−6 molecules. This differs dramatically from the localization observed in disordered inorganic semiconductors, such as hydrogenated amorphous silicon,[25] where only states near the energy gap are strongly localized, while all other states in the bands show significant delocalization over the entire structure. Thus, the conventional bandlike description is not appropriate for amorphous PFOs.

Interestingly, the number of moderately delocalized states (PR ≥ 1.5) is larger near the edge of the VB than the CB, although the states in the CB are more dense than in the VB. Thus, in the energy ranges of ~0.2 eV from HOMO, indicated by red brackets in Figure 4a, there are six states that are delocalized over two molecules (PR ≥ 1.5), while in the same energy range from the LUMO all states are localized (PR < 1.5). For the energy range of ~0.3 eV from HOMO (LUMO) there are

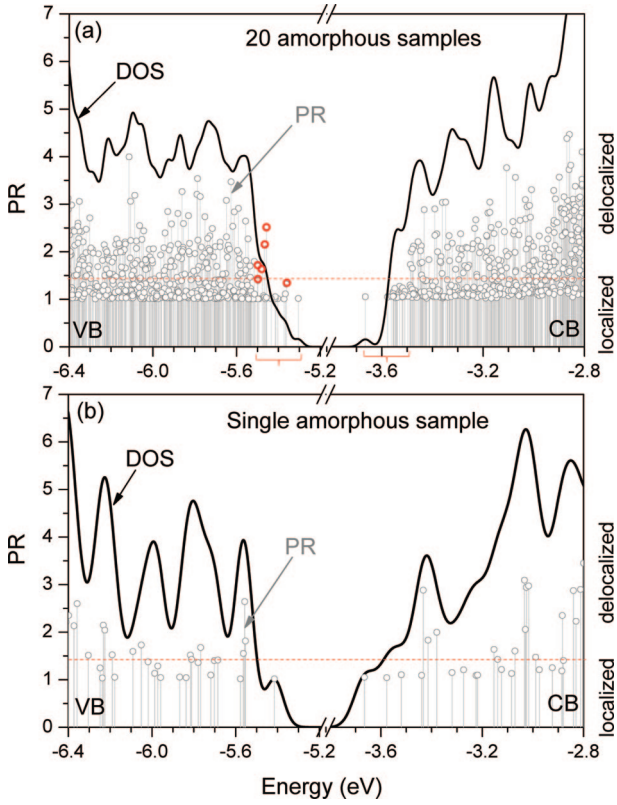

Figure 4. Calculated density of states (DOS) and participation ratios (PR). (a) Averaged data for 20 different equilibrium configurations of amorphous PFO aggregates. (b) Data for a single amorphous sample. The DOS values are shown in arbitrary units obtained by adding Gaussian broadening to the respective orbital energies. The PR approaching to 8 corresponds to the maximal delocalized orbital, when its charge density is distributed over all eight PFO chains. The smaller is the PR, the stronger is the localization of an orbital. The dash red line shows the border between localized (under the line, PR < 1.5) and delocalized (above the line, PR ≥ 1.5) states. Surprisingly, there are a lot of localized states deep inside in the valence (VB) and the conduction (CB) bands. Although edges of both the VB and the CB near the band gap, indicated by the red brackets, mostly show localized states, there are a few delocalized orbitals in the VB (red circles) and not one in the CB. This assumes more probable formation of trap states—orbitals that are strongly localized on a single PFO chain—for electrons rather than for holes.

24 delocalized states in the edge of the VB and only 16 delocalized states in the edge of the CB. An analysis of the geometries and torsional angles of PFOs in different aggregates shows that PFO molecules with two or more large torsions have a tendency to have their orbitals deeper in the VB of the aggregate (far from the HOMO), while their LUMOs are closer in energy to the LUMO of the aggregate. Nonetheless, since configurations with large torsions are common, both intermolecular and conformational disorder in amorphous PFO aggregates lead to the appearance of strongly localized states with PR < 1.5 deep inside the CB and VB, as shown in Figure 4.

CONCLUSIONS

In summary, we have studied the connection between electronic delocalization and intermolecular interactions/conformational disorder in amorphous PFO aggregates. By combining classical molecular dynamics with modified FF and quantum-mechanical DFT simulations, our computational methodology allows us to address packing morphology effects on electronic structure of large disordered systems. Localization of calculated electronic states is further investigated using participation ratio analysis, an approach commonly used for disorder characterization in inorganic semiconductors.[25] We find that intermolecular interactions allow for nearly planar configurations of disordered PFO chains (small torsion angles). This rationalizes the formation of the β phase in addition to the α phase in PFO materials. Our calculations show that the energy of the electron state (unnoccupied orbital) is more sensitive to the variation of the torsional angles compared to the hole state (occupied orbital). Consequently, we observe strongly localized states near the edge of the CB to be more probable than those near the edge of the VB. This may likely lead to the formation of electron trap states, which is similar to what has been found previously for poly-*p*-phenylene (PPV),[19] and might explain a much higher mobility of holes than electrons in PFO materials. Finally, our simulations show that the nature of disorder and its impact on charge-carrier localization in amorphous PFOs differ dramatically from those of disordered inorganic semiconductors, such as amorphous silicon. Electronic levels of disordered PFOs are mostly localized on a single molecule not only for the states near the band edges, but also deep inside the bands. Thus, theoretical methodologies postulating a bandlike description for mobility calculations may not be appropriate for amorphous fluorenes.

METHODOLOGY

Isolated PFO Chain. Each PFO chain in the simulated materials is constructed from five repeated units. Optimal structures of an isolated PFO pentamer are schematically presented in Figure 1a,b, showing molecules with and without octyl groups (C_8H_{17}), respectively. The geometry of isolated PFO chains was calculated in vacuum using DFT with the B3LYP hybrid functional and 6-31+G^* basis set, as implemented in the Gaussian 03 package.[27] The torsion angle between each monomer in the optimized PFO is close to 37° and is independent of the presence of octyl-side groups. Such a relatively large torsional angle leads to a helix-like conformation of PFO molecules. The helical tendency is more pronounced for longer chains (16 units, not shown), which is in good agreement with thin film electron diffraction studies on a closely related material,[28] where it was found that a molecule of poly(9,9-bis(2-ethylhexyl)-fluorene-2,7-diyl)(PF2/6) adopts a helical (5 monomers on two turns) conformation.

Geometry Optimization of Amorphous Samples. The amorphous phase of PFO is simulated using 20 different random configurations (snapshots) of disordered finite cells using an annealing procedure which is based on MM3-2000 FF[29,30] as implemented in the TINKER code.[31] Although this FF was created for calculations of a variety of organic molecules, it was not parameterized

specifically for PFO oligomers. Following ref 19 we reparameterized the height and the shape of the torsional barrier (V_1, V_2, and V_3 parameters[32]) using the B3LYP-dependence of the total electronic energy on the torsional angle between two central biphenyl units in the isolated PFO chain. The latter reference potential has a negligible dependence on the presence of octyl groups and the number of repeat units in the PFO chain (see Figure 2a). Thus, the modified MM3-2000 FF can be used for PFO molecules, providing results for geometry conformations of fluorenes with an accuracy comparable to that of DFT calculations. Because the alkyl side chains play a key role in the polymer packing determining the spatial distance between chains, octyl groups are preserved during the FF simulations of the amorphous PFO aggregates, as shown in Figure 1c,e. From these simulations, the 20 snapshots are extracted, each containing eight PFO pentamers in a periodically repeated simulation cell of size about $3 \times 3 \times 3$ nm^3. Periodic boundary conditions (PBC) replicate a simulation cell and establish the continuity of molecules inside each cell. For the annealing simulations,[19] eight PFO pentamers have been initially randomly distributed at extremely low density (0.01 g/cm^3). Then samples are heated to 2000 K and cooled to 1000 K at applied pressure in order to reach the experimental density of glassy α phase of PFO films ($\sim$1.041 g/mL.[33]). At this density the volume of the simulation cell is kept constant and the temperature is gradually cooled to 0 K. Finally, the amorphous geometries are extracted, and statistical sampling is generated by repeating the above annealing procedure.

The total number of atoms in the cell (Figure 1c,e) is 2776, which is manageable for FF simulations, but is problematic for quantum chemical calculations. To reduce the number of atoms in the cell, while preserving the main physical properties of the system, the octyl groups have been replaced by hydrogens. This reduces the number of atoms to 856, allowing for DFT electronic structure calculations. Figure 1d,f show the same snapshot of the optimized amorphous PFO material as in Figure 1c,e, but without the octyl groups. As can be seen from Figure 1d,e, the intermolecular spacing between PFO chains is relatively large; the averaged distance between biphenyl rings in the neighboring PFO chains is around 3.7 Å. This presumes relatively weak $\pi-\pi$ interactions between nearest chains, compared to PPV amorphous aggregates, where the averaged intermolecular distance is calculated to be around 3 Å.[19]

Electronic Structure Calculations. The electronic structure calculations of the isolated PFO molecules and disordered PFO aggregates are performed with the VASP code.[34] This code utilizes PBC DFT using a plane wave basis set. The core electrons are simulated using the Vanderbilt pseudopotentials,[35] while all valence electrons are treated explicitly. The generalized gradient approximation (GGA) functional due to Perdew and Wang (PW91)[36] is used to account for the electron exchange and correlation effects. Because of the large size of the simulation cells (typically 30 Å on each side), the Γ point sampling of the Brillouin zone is adequate. We checked that adding an extra two or three k points in each direction did not change the energy of electronic states in a range of 2 eV above and below the energy gap. Use of the GGA leads to underestimated energy gap values. This failure is typical for GGA calculations, stemming ultimately from the incomplete elimination of self-interaction by these functionals.[37] However, we are primarily interested in relative energies of electronic levels and not in the absolute value of the energy gap. The effect of octyl groups on the electronic structure of PFOs was estimated by comparison of the electronic energies of the isolated PFO pentamer with and without octyl groups. The electronic energy levels of both molecules coincided with an accuracy up to the third decimal place proving a negligible impact of octyl chains on the energy level spectrum of the PFOs.

Acknowledgment. This work was supported by the DOE Office of Basic Energy Sciences under Work Proposal Number 08SCPE973. LANL is operated by Los Alamos National Security, LLC, for the National Nuclear Security Administration of the U.S. Department of Energy under contract DE-AC52-06NA25396.

Supporting Information Available: Details of the computational approach to electron localization in amorphous PFO aggregates. This material is available free of charge *via* the Internet at http://pubs.acs.org.

REFERENCES AND NOTES

1. Malliaras, G.; Friend, R. An Organic Electronics Primer. *Phys. Today* **2005**, *58*, 53–58.
2. Redecker, M.; Bradley, D.; Inbasekaran, M.; Woo, E. P. Nondispersive Hole Transport in an Electroluminescent Polyfluorene. *Appl. Phys. Lett.* **1998**, *73*, 1565–1567.
3. Kreouzis, T.; Poplavskyy, D.; Tuladhar, S. M.; Campoy-Quiles, M.; Nelson, J.; Campbell, A. J.; Bradley, D. D. C. Temperature and Field Dependence of Hole Mobility in Poly(9,9-dioctylfluorene). *Phys. Rev. B* **2006**, *73*, 235201–235204.
4. Sims, M.; Bradley, D.; Ariu, M.; Koeberg, M.; Asimakis, A.; Grell, M.; Lidzey, D. Understanding the Origin of the 535 nm Emission Band in Oxidized Poly(9,9-dioctylfluorene): The Essential Role of Inter-chain/Inter-segment Interactions. *Adv. Funct. Mater.* **2004**, *14*, 765–781.
5. Franco, I.; Tretiak, S. Electron-Vibrational Dynamics of Photoexcited Polyfluorenes. *J. Am. Chem. Soc.* **2004**, *126*, 12130–12140.
6. Neher, D. Polyfluorene Homopolymers: Conjugated Liquid-Crystalline Polymers for Bright Blue Emission and Polarized Electroluminescence. *Macromolecules* **2001**, *22*, 1366–1385.
7. Gross, M.; Müller, D.; Nothofer, H.; Scherf, U.; Neher, D.; Bräuchle, C.; Meerholz, K. Improving the Performance of Doped π -Conjugated Polymers for Use in Organic Light-Emitting Diodes. *Nature* **2000**, *405*, 661–664.
8. Virgili, T.; Marinotto, D.; Lanzani, G.; Bradley, D. Ultrafast Resonant Optical Switching in Isolated Polyfluorenes Chains. *Appl. Phys. Lett.* **2005**, *86*, 091113−091116.
9. Sirringhaus, H.; Wilson, R.; Friend, R. H.; Inbasekaran, M.; Wu, W.; Woo, E. P.; Grell, M.; Bradley, D. Mobility Enhancement in Conjugated Polymer Field-Effect Transistors through Chain Alignment in a Liquid-Crystalline Phase. *Appl. Phys. Lett.* **2000**, *77*, 406–408.
10. Heliotis, G.; Xia, R.; Turnbull, G.; Andrew, P.; Barnes, W.; Samuel, I.; Bradley, D. Emission Characteristics and Performance Comparison of Polyfluorene Lasers with One- and Two-Dimensional Distributed Feedback. *Adv. Funct. Mater.* **2004**, *14*, 91–97.
11. Cadby, A.; Lane, A.; Mellor, H.; Martin, S.; Grell, M.; Giebeler, C.; Bradley, D.; Wohlgenannt, M.; An, C.; Vardeny, Z. Film Morphology and Photophysics of Polyfluorene. *Phys. Rev. B* **2000**, *62*, 15604–15609.
12. Como, E. D.; Becker, K.; Feldmann, J.; Lupton, J. M. How Strain Controls Electronic Linewidth in Single β -Phase Polyfluorene Nanowires. *Nano Lett.* **2007**, *7*, 2993–2998.
13. Prins, P.; Grozema, F.; Nehls, B.; Farrell, T.; Scherf, U.; Siebbeles, L. Enhanced Charge-Carrier Mobility in Beta-Phase Polyfluorene. *Phys. Rev. B* **2006**, *74*, 113203–113207.
14. Athanasopoulos, S.; Kirkpatrick, J.; Martinez, D.; Frost, J.; Foden, C.; Walker, A.; Nelson, J. Predictive Study of Charge Transport in Disordered Semiconducting Polymers. *Nano Lett.* **2007**, *7*, 1785–1788.
15. Lupton, J. Smaller-Faster-Brighter: Developing Optical Probes of the Future. *ChemPhysChem* **2003**, *4*, 555–558.
16. Beljonne, D.; Pourtois, G.; Silva, C.; Hennebicq, E.; Herz, L.; Friend, R.; Scholes, G.; Setayes, S.; Müllen, K.; Brédas, J. Interchain vs. Intrachain Energy Transfer in Acceptor-Capped Conjugated Polymers. *Proc. Natl. Acad. Sci. U.S.A.* **2002**, *99*, 10982–10987.
17. Barbara, P. F.; Chang, W. S.; Link, S.; Scholes, G. D.; Yethiraj, A. Structure and Dynamics of Conjugated Polymers in Liquid Crystalline Solvents. *Annu. Rev. Phys. Chem.* **2007**, *58*, 565–584.
18. Tretiak, S.; Saxena, A.; Martin, R. L.; Bishop, A. R. Conformational Dynamics of Photoexcited Conjugated Molecules. *Phys. Rev. Lett.* **2002**, *89*, 097402−097405.

19. Yang, P.; Batista, E. R.; Tretiak, S.; Saxena, A.; Martin, R. L.; Smith, D. L. Effect of Intramolecular Disorder and Intermolecular Electronic Interactions on the Electronic Structure of Poly-*p*-phenylene Vinylene. *Phys. Rev. B* **2007**, *76*, 241201–241204.
20. Coropceanu, V.; Cornil, J.; da Silva Filho, D.; Olivier, Y.; Silbey, R.; Bredas, J.-L. Charge Transport in Organic Semiconductors. *Chem. Rev.* **2007**, *107*, 926–952.
21. Brédas, J. L.; Cornil, J.; Beljonne, D.; dos Santos, D. A.; Shuai, Z. Excited-State Electronic Structure of Conjugated Oligomers and Polymers: A Quantum-Chemical Approach to Optical Phenomena. *Acc. Chem. Res.* **1999**, *32*, 267–276.
22. Ruini, A.; Caldas, M. J.; Bussi, G.; Molinari, E. Solid State Effects on Exciton States and Optical Properties of PPV. *Phys. Rev. Lett.* **2002**, *88*, 206403–206404.
23. Cornil, J.; Beljonne, D.; Calbert, J. P.; Brédas, J. L. Interchain Interactions in Organic π -Conjugated Materials: Impact on Electronic Structure, Optical Response, and Charge Transport. *Adv. Mater.* **2007**, *13*, 1053–1067.
24. Tretiak, S.; Saxena, A.; Martin, R. L.; Bishop, A. R. Interchain Electronic Excitations in Poly(phenylene-vinylene) (PPV) Aggregates. *J. Phys. Chem. B* **2000**, *104*, 7029–7037.
25. Abtew, T.; Drabold, D. Hydrogen Dynamics and Light-Induced Structural Changes in Hydrogenated Amorphous Silicon. *Phys. Rev. B* **2006**, *74*, 085201−085205.
26. Ono, Y; Ohtsuki, T.; Kramer, B. Inverse Participation Number and Fractal Dimensionality of Electronic States in a Two Dimensional System in Strong Perpendicular Magnetic Field. *J. Phys. Soc. Jpn.* **1989**, *58*, 1705–1716.
27. Frisch, M. J.; Trucks, G. W.; Schlegel, H. B.; Scuseria, G. E.; Robb, M. A.; Cheeseman, J. R.; Montgomery, J. A., Jr.; Vreven, T.; Kudin, K. N.; Burant, J. C.; *et al*. Gaussian-03, revision 0.02; Gaussian, Inc.: Wallingford, CT, 2004.
28. Lieser, G.; Oda, M.; Miteva, T.; Meisel, A.; Nothofer, H.-G.; Scherf, U.; Neher, D. Ordering, Graphoepitaxial Orientation, and Conformation of a Polyfluorene Derivative of the 'Hairy-Rod' Type on an Oriented Substrate of Polyimide. *Macromolecules* **2000**, *33*, 4490–4495.
29. Allinger, N.; Yuh, Y.; Lii, J.-H. Molecular Mechanics. The MM3 Force Field for Hydrocarbons. *J. Am. Chem. Soc.* **1989**, *111*, 8551–8566.
30. Lii, J.-H.; Allinger, N. L. Molecular Mechanics. The MM3 Force Field for Hydrocarbons: The van der Waals' Potentials and Crystal Data for Aliphatic and Aromatic Hydrocarbons. *J. Am. Chem. Soc.* **1989**, *111*, 8576–8582.
31. Ponder, J. W. *TINKER: Software Tools for Molecular Design,* Version 3.8; Washington University School of Medicine: St. Louis, MO, 2000.
32. Tafipolsky, M.; Schmid, R. Theoretical Determination of Accurate Rate Constants: Application to the Decomposition of a Single-Molecule Precursor. *Surf. Coat. Technol.* **2007**, *201*, 8818–8824.
33. Chen, S.; Su, A.; Su, C.; Chen, S. Crystalline Forms and Emission Behavior of Poly(9,9-di-*n*-octyl-2,7-fluorene). *Macromolecules* **2005**, *38*, 379–385.
34. Kresse, G.; Furtmüller, J. Efficient Iterative Schemes for *ab Initio* Total-Energy Calculations Using a Plane-Wave Basis Set. *Phys. Rev. B* **1996**, *54*, 11169–11174.
35. Vanderbilt, D. Soft self-Consistent Pseudopotentials in a Generalized Eigenvalue Formalism. *Phys. Rev. B* **1990**, *41*, 7892–7896.
36. Perdew, J. P. *Electronic Structure of Solids;* Ziesche, P., Eschrig, H., Eds.; Akademie Verlag: Berlin, 1991.
37. Peralta, J. E.; Heyd, J.; Scuseria, G. E; Martin, R. L. Spin-Orbit Splittings and Energy Band Gaps Calculated with the Heyd-Scuseria-Ernzerhof Screened Hybrid Functional. *Phys. Rev. B* **2006**, *74*, 073101−073105.